Journal of Robotics and Control (JRC)
Volume 3, Issue 3, May 2022
ISSN: 2715-5072, DOI: 10.18196/jrc.v3i3.14750

Autonomous Movement Control of Coaxial Mobile Robot based on Aspect Ratio of Human Face for Public Relation Activity Using Stereo Thermal Camera

Muhammad Ilhamdi Rusydi [1], Aulia Novira [2], Takayuki Nakagome [3], Joseph Muguro [4], Rio Nakajima [5], Waweru Njeri [6], Kojiro Matsushita [7], and Minoru Sasaki [8*]
[1,2] Department of Electrical Engineering, Faculty of Engineering, Universitas Andalas, Padang City, Indonesia
[3] Aisin Software Co. Ltd.
[4] Intelligent Production Technology Research & Development Center for Aerospace (IPTeCA), Tokai National Higher Education and Research System, Japan
[4,6] Center for Robotics and Biomedical Engineering, Department of Electrical & Electronic Engineering, Dedan Kimathi University of Technology, Private Bag, Nyeri 10143, Kenya
[4,5,7,8] Department of Mechanical Engineering, Faculty of Engineering, Gifu University, 1-1 Yanagido, Gifu, 501-1193, Japan
Email: sasaki@gifu-u.ac.jp
[*]Corresponding author

***Abstract*—In recent years, robots that recognize people around them and provide guidance, information, and monitoring have been attracting attention. The mainstream of conventional human recognition technology is the method using a camera or laser range finder. However, it is difficult to recognize with a camera due to fluctuations in lighting 1), and it is often affected by the recognition environment such as misrecognition 2) with a person's leg and a chair's leg with a laser range finder. Therefore, we propose a human recognition method using a thermal camera that can visualize human heat. This study aims to realize human-following autonomous movement based on human recognition. In addition, the distance from the robot to the person is measured with a stereo thermal camera that uses two thermal cameras. A coaxial two-wheeled robot that is compact and capable of super-credit turning is used as a mobile robot. Finally, we conduct an autonomous movement experiment of a coaxial mobile robot based on human recognition by combining these. We performed human-following experiments on a coaxial two-wheeled robot based on human recognition using a stereo thermal camera and confirmed that it moves appropriately to the location where the recognized person is in multiple use cases (scenarios). However, the accuracy of distance measurement by stereo vision is inferior to that of laser measurement. It is necessary to improve it in the case of movement that requires more accuracy.**

Keywords—Coaxial mobile robot; Human following robot; Recognition; Stereo thermal camera.

I. INTRODUCTION

Integration of robotics in modern societies is a promising venture that has gained popularity in the recent past. Robotics have been integrated into automation, transportation, medical fields, defense systems, rehabilitation, and rehabilitation [1]–[5]. The pervasiveness of robot integration is seen in the uptake of robots in living and working spaces which seeks to avail advanced human-robot coexistence to enhance the quality of life [6]–[9].

There are broadly two human-robot models: collaborative [10]–[13] and cooperative robots [1], [12]–[17]. In a cooperative robot system, the human and the robot work simultaneously on a task. On the hand, collaborative robots work hand-in-hand with a human to accomplish a goal. In either of these scenarios, human and environment detection is paramount. In addition, indoor robots (share spaces with humans) have restrictions on form factors and maneuverability to ensure safety [18]–[20].

In literature, the following human robots have been investigated using different approaches. Neural network bases recognition and tracking, cameras, lidar, ultrasonic sensors, infrared sensors, voice recognition, rf-tags, and laser range finder (LRF) sensor, amongst others [21]–[26]. Such systems are deployed in indoor navigation robots [27], social communication robots [28], [29], and security robots [30], [31] that recognize people around them and provide guidance, crowd-control, and safety monitoring and interaction with COVID-19 patients in the recent past [32]–[34].

Cameras and laser-based systems have gained popularity due to accuracy and increasing computing/processing power. However, the camera-based system is challenged by environmental illuminance levels and or the presence of infrared rays, as is the case in infrared cameras [35], [36]. On the other hand, the laser-based system suffers from erroneous/misrecognition of similar-shaped objects. For example, the laser-based system misrecognizes human legs and chairs from the scan data or other objects with a similar shape [37], [38]. As a remedy, a hybrid of laser-based and camera-based systems is adopted in literature to compensate for the individual system's weak points.

This research utilizes a mobile robot equipped with a thermal camera-based human-tracking algorithm system to realize autonomous human-following robots. In the

architecture, two thermal cameras are used to measure the distance of the human [39]. A thermal camera is a camera that visualizes the heat energy emitted from an object and displays the temperature distribution in real-time [40]–[42]. This camera is used to measure the temperature of a person's face and recognize the person. In addition, we try to measure the distance from the camera to a person by mounting a thermal camera on a drive-type stereo camera and moving from the measured data to the front of the person. We employ a coaxial robot as it has been shown to be ideal in indoor and constrained spaces as it can achieve pivot turning and has a small form factor.

The purpose of this research was originally to carry out public relations activities by hand, such as standing with a signboard and handing out leaflets. In addition, public relations may be carried out by installing posters and signboards that do not require labor costs. However, with such public fixed-type ties, it is impossible to carry out public relations efficiently because it is not noticeable to people and is located with few people. Therefore, the main contribution of this research is by carrying out public relations activities using autonomous mobile robots instead of humans. This study uses a stereo thermal camera to implement the human recognition system in the mobile robot. To show the system's effectiveness proposed in this study, we conducted a running experiment in which people recognize and move.

II. MATERIAL AND METHODS

Fig. 1 shows the system of autonomous coaxial mobile robot. This robot has the ability to detect and follow a human. The human face is the input of the camera. Human faces are rounded and detected based on aspect ratio. The positions of the human to the robot are calculated as the input to move the coaxial robot.

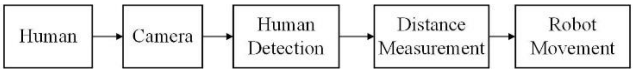

Fig. 1. Autonomous coaxial mobile robot system

A. Proposed Configuration System

Fig. 2 illustrates the configuration employed in the research. We used two thermal cameras (FLIR C2 Teledyne®) with each camera attached to servomotors. The camera has a steerable 2-DoF (up-down, side-side) movement to orient the view for accurate depth and human detection. The details of operations will be explained in a subsequent section. A laptop computer performs image processing of the thermal camera and control of the robot (Let's Note: S10 with i5 processor).

We designed a two-wheel coaxial robot and attached the two thermal cameras as shown in Fig. 3. The coaxial robot base is used to carry the processing PC as well as the sensors. We used Rx-64 servomotor for the wheel and AX-12A servomotors for orienting the cameras. The specifications of the camera and motor are shown in Fig. 4, Fig. 5, Table 1, and Table 2.

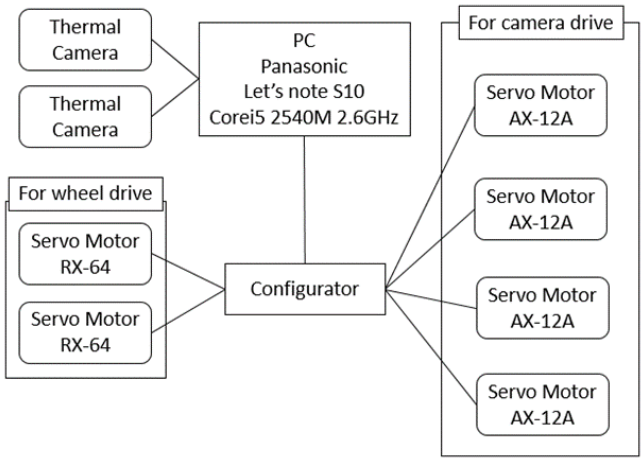

Fig. 2. The configuration system of an autonomous coaxial mobile robot is based on a thermal camera.

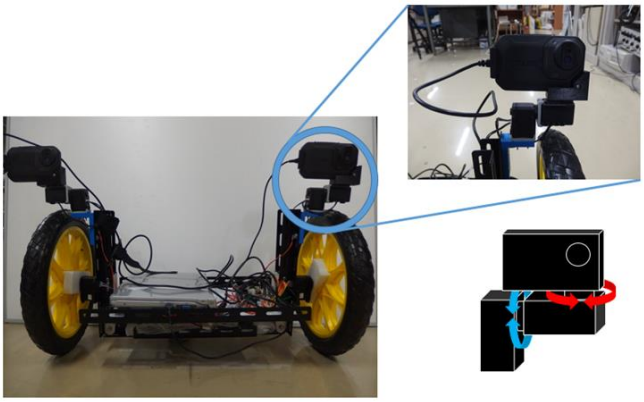

Fig. 3. External view of the two-wheeled robot

TABLE I. CAMERA AND LRF SPECIFICATIONS

Camera System (FLIR C2)	
IR sensor	80×60
Thermal Sensitivity	0.1℃
Field of view	41°×31°
Image frequency	9Hz
Temperature range	-10℃ ～ +150℃
LRF System (UTM-30LX(HOKUYO))	
Power-supply voltage	DC12V
Distance range	0.1～30[m]
Measurement range	270[deg]
Distance accuracy	0.1～10[m]: ∓30[mm]
Measurement accuracy	10～30[m]: ∓50[mm]
Step angle	0.25[deg]

Fig. 4. Thermal camera (FLIR C2) and LRF sensor (UTM-30LX (HOKUYO))

TABLE II. SERVO MOTOR SPECIFICATION

Specification	DYNAMIXEL AX-12A	DYNAMIXEL RX-64
Stall Torque	1.5N · m	52kgf · cm
Voltage	9～12V	12～21V
Running Degree	0～300°	Endless Turn
Resolution	0.29°	0.29°

(a) (b)

Fig. 5. Servomotors used (a) dynamixel AX 12 A (b) dynamixel RX-64

The mechanism of the coaxial robot can be thought of as an inverted pendulum with a center of gravity above the robot body [43], as shown in Fig. 6(a), making the robot unstable [44]. In this case, posture control is needed to stabilize the system (altitude control). If an abnormality occurs in the hardware or software, or if an external force exceeds the control limit is applied, the altitude cannot be maintained stably, and the robot falls.

We have been researching how to maintain a stable posture by using physical restoring force to stabilize the posture of stable coaxial mobile robots in our laboratory. By arranging the center of gravity below the center of rotation of the wheels, as shown in Fig. 6(b), it is possible to maintain the upright posture only by physical force with high reliability. Further details can be obtained in previous research conducted by our lab [45], [46]. In this study, the system shown in Fig. 6(b) is utilized in the design of a coaxial mobile robot.

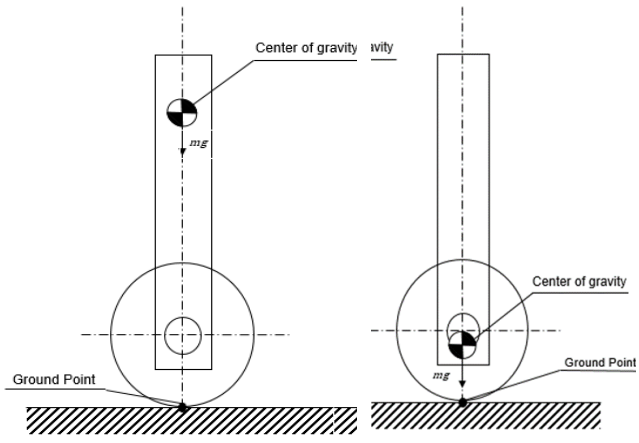

(a) (b)

Fig. 6. Two-wheeled robot construction (a) Inverted pendulum system, (b) Gravity stabilized inverted pendulum

B. Human Detection Algorithm

In this research, we utilize cameras to detect humans and calculate the distance between the system and the target (person). The workflow is shown in Fig. 7. We acquire a thermal image of a person from a thermal camera and recognize the person [47]. Therefore, we explain human recognition from the acquired thermal image, distance measurement from the camera to the person, and movement control of the coaxial mobile robot.

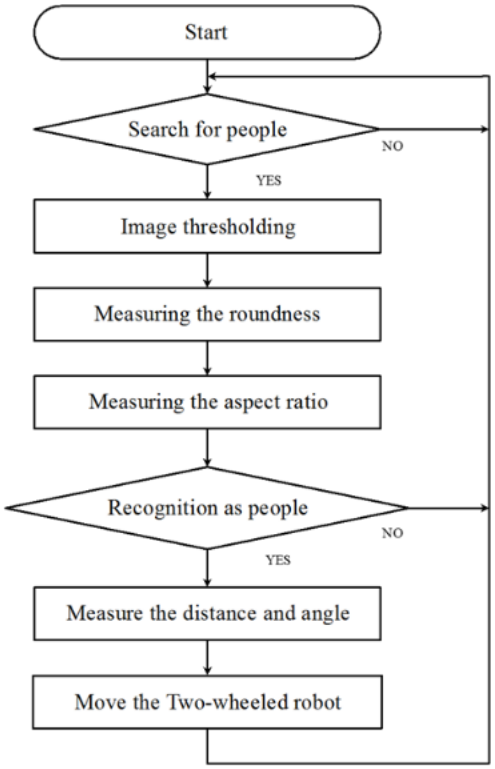

Fig. 7. Flow chart of the proposed system.

Human Detection Algorithm

The acquired image is binarized by the discriminant analysis method. The discriminant analysis method automatically determines the threshold value t [48]–[50] so that the separation of the two classes is the best [18][47]. The method workings are as shown in Fig. 8.

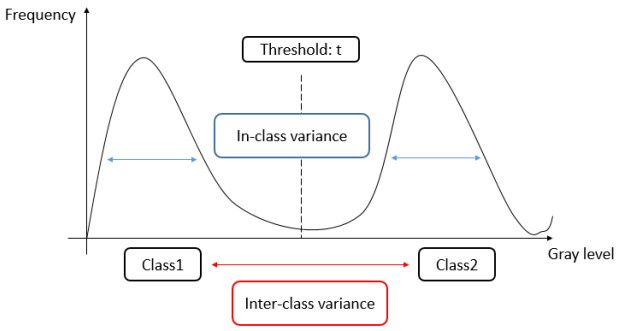

Fig. 8. Flow chart of the proposed system.

Assuming that the threshold value is t, the range of cardinality values from 0 to t-1 is class 1, and the range of t to 255 is class 2. At this time, the number of pixels is n_1, n_2 the average of the density values is $\bar{f_1}$, $\bar{f_2}$ the variance is σ_1^2,

σ_2^2 and the number of pixels with density f is n_f. The distribution of each class is calculated by (1) and (2).

$$\sigma_1^2 = \frac{\sum_{f=0}^{t} n_f (f - \bar{f}_1)^2}{n_1 + n_2} \quad (1)$$

$$\sigma_2^2 = \frac{\sum_{f=t}^{255} n_f (f - \bar{f}_2)^2}{n_1 + n_2} \quad (2)$$

Next, the intra-class variance σ_W^2, which indicates the spread of concentration values within each class, and the inter-class variance σ_B^2 which indicates the spread of class 1 and class 2, are obtained by (3) and (4).

$$\sigma_W^2 = \frac{n_1\sigma_1^2 + n_2\sigma_2^2}{n_1 + n_2} \quad (3)$$

$$\sigma_B^2 = \frac{n_1(\bar{f}_1 - \bar{f}_F)^2 + n_2(\bar{f}_2 - \bar{f}_F)^2}{n_1 + n_2} \quad (4)$$

where, $\bar{f}_F$ is the average of the density values of all pixels. The best separation between classes is when the variance ratio σ_B^2/σ_W^2 is maximized. Therefore, the larger the variance between the classes and the smaller the variance within the class, the better the separation. The optimum threshold value can be obtained by finding the threshold value t that maximizes this dispersion ratio. In this study, the images obtained from the thermal camera are binarized by this discriminant analysis method.

Circularity is often used as a quantity to measure the shape of a region, and it is possible to judge whether it is close to a circle or not by a numerical value [16]. This circularity can be calculated by (5). Let R is the circularity, S is the region's area, and L is the perimeter of the region.

$$R = 4\pi\frac{S}{L^2} \quad (5)$$

If the circularity is a perfect circle, R = 1, and if it is closer to a circle, the circularity becomes higher. The human face is rounded and has a shape close to a circle. Therefore, the human face is judged using this circularity in this research, as shown in Fig. 8.

(a) (b)

Fig. 9. Face recognition by the roundness (a) Thermal camera detection of a face (b) detected face using circularity

Aspect ratio is often used to obtain human characteristics [51]. Human faces also have a feature that is basically longer in the vertical direction than in the horizontal direction, as illustrated in Fig. 10. The ratio of the vertical to horizontal directions of the face is calculated and used for human face recognition based on the aspect ratio feature.

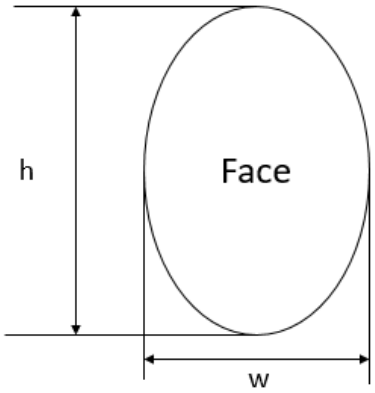

Fig. 10. Face recognition by the aspect ratio

When the height of a person's face is h, and the width is w, the aspect ratio of the face is A. This is represented by (6).

$$A = \frac{w}{h} \quad (6)$$

Considering that the human face is longer in the vertical direction than in the horizontal direction, it is considered that the aspect ratio A does not exceed 1. A human face is measured using this aspect ratio.

After recognizing people, if there are multiple people, the center point of those people must be calculated, and the angle and depth of those points must be calculated from the stereo camera. Therefore, the position of the center is calculated using the K-means algorithm [2], [52], [53]. The procedure of this algorithm with K clusters is as follows.

a. Select any K attribute value vectors as the center of the initial cluster. Let this be $Y_1(1), Y_2(2), \ldots, Y_K(n)$.

b. Classify into subset $S_1(n), S_2(n), \ldots, S_K(n)$. (n: number of times the procedure is repeated) corresponding to the cluster centers $Y_1(n), Y_2(n), \ldots, Y_K(n)$ for all attribute vectors {X} by (7).

$$d_l = \min_{j \in N_K}\{d_j\} \quad [X \in S_l, N_K \triangleq \{1,2,\ldots,K\}] \quad (7)$$

where, d_j is the distance between X and $Y_j(n)$ is calculated by (8).

$$d_j \triangleq \|X - Y_j(n)\| \quad (8)$$

c. For each subset, find the new cluster centers $Y_1(n+1), Y_2(n+1), \ldots, Y_K(n+1)$ by (9). Also, N_l is the original number of the set $S_l(n)$.

$$Y_l(n+1) = \frac{1}{N_l}\sum_{X \in S_l(n)} X \quad (9)$$

d. If Equation (10) holds for all clusters, this algorithm is terminated. If not, return to step (c) and repeat.

$$Y_l(n+1) = Y_l(n), l \in N_K \quad (10)$$

This algorithm is used to identify the positions of the centers of gravity of multiple people.

C. Distance Measurement

Humans can obtain the depth of the object based on the information obtained from the two left and right visions. This is because there is a difference in the information obtained from the left and right, and the parallax is used to grasp the stereoscopic effect and distance. This measurement method has the same principle as triangulation. This research uses a drive-type stereo camera equipped with a servomotor in each camera instead of a fixed stereo camera. In the case of a fixed stereo camera, only the object presented ahead of the camera can be detected. Further, depth becomes an issue as perspective changes. With a driven stereo camera, it is possible to search not only the front of the camera but also the sides by rotating the camera with a motor. The mechanism we employed to determine the X and Y coordinates of the detected faces is described further.

2D Distance Measurement

Let the coordinates of the object (human face shown in yellow) in Fig. 11 be (X, Y, Z). First, the image is acquired, and the face is centered using a servomotor. At that time, the angle (α, β) obtained from the servo motor is used. The angle is positive on the left side of the center of each axis and negative on the right side.

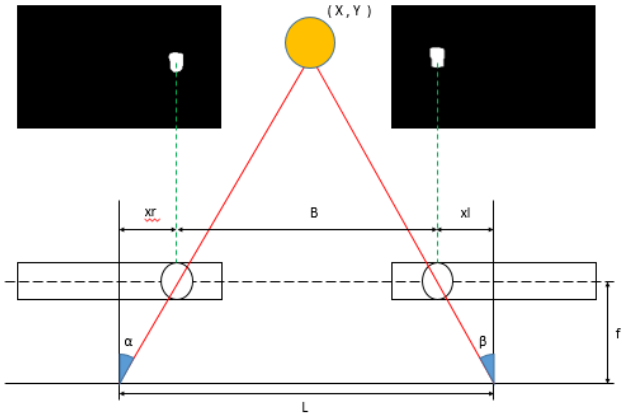

Fig. 11. Method of distance measurement by the stereo camera

The depth (Y) to the object can be obtained from the relationship of triangles using (11).

$$Y : Y - f = L : B$$

$$\Leftrightarrow \quad Y = \frac{Lf}{L - B} \tag{11}$$

Here unknown parameter B is (12)

$$B = L - xr - xl \tag{12}$$

Where xr and xl can be represented by angles α and β by (13) and (14).

$$xr = ftan(-\alpha) \tag{13}$$

$$xl = ftan(\beta) \tag{14}$$

From these formulas (15), the depth (Y) can be obtained.

$$Y = \frac{Lf}{L - \{L - ftan(-\alpha) - ftan(\beta)\}}$$

$$\Leftrightarrow \quad Y = \frac{L}{-\tan(\alpha) + \tan(\beta)} \tag{15}$$

Next, we need to find the X coordinate to show where the object is. Based on the camera on the left, if we move the object by X units from the previous position, as shown in Fig 12, we can derive the expression from Y and the new angles of the servo motor.

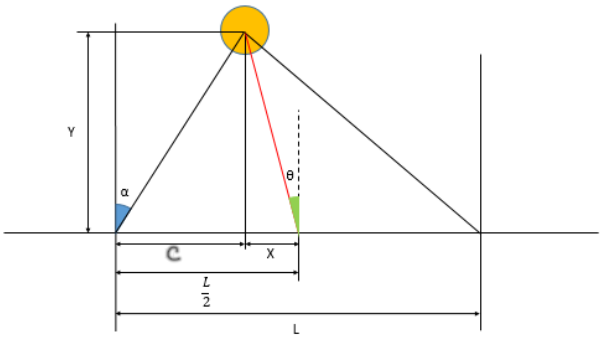

Fig. 12. The movement of the reference point

The new X coordinate of the object is C (note the sign of α) when the left camera is used as a reference. The relationship is represented by (16).

$$X = \frac{L}{2} - C \tag{16}$$

Expressing C in terms of trigonometric relations, we obtain (17).

$$C = Y\tan(-\alpha) \tag{17}$$

Replacing (17) in (16), we get (18).

$$X = \frac{L}{2} - Y\tan(\alpha)$$

$$\Leftrightarrow \quad X = \frac{L}{2} - \frac{L}{-\tan(\alpha) + \tan(\beta)}\tan(\alpha) \tag{18}$$

From this, the angle (θ) from the center of the stereo camera to the object can be obtained (19).

$$\tan(\theta) = \frac{X}{Y}$$

$$\Leftrightarrow \quad \theta = \tan^{-1}\frac{X}{Y}$$

$$\Leftrightarrow \quad \theta = \tan^{-1}\frac{\frac{L}{2} - \frac{L}{-\tan(\alpha) + \tan(\beta)}\tan(\alpha)}{\frac{L}{-\tan(\alpha) + \tan(\beta)}}$$

$$\Leftrightarrow \quad \theta = \tan^{-1}\frac{-3\tan(\alpha) + \tan(\beta)}{2} \tag{19}$$

From the above, the distance and position from the stereo camera to the object can be measured. The data obtained by this stereo camera is used to control the movement of the coaxial mobile robot.

3D Distance Measurement

The distance was measured on a two-dimensional plane earlier. However, when mounted on a coaxial mobile robot,

the position of the camera is low, and the position of the face cannot be measured, so the camera must be turned upward. Therefore, the distance is measured by moving the camera up and down using a servo motor, as shown in Fig. 13.

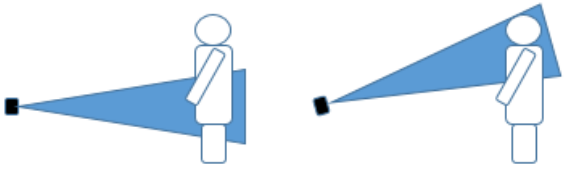

Fig. 13. The orientation of the camera

The method of measuring the distance is the same as that of the quadratic plane, and the distance is measured by using the coordinates (X, Y) and the angle of the servo motor that tilts the camera up and down. The value of depth (Y) changes by giving an angle, as shown in Fig. 14. Therefore, the coordinates of the object are corrected, and the distance is estimated.

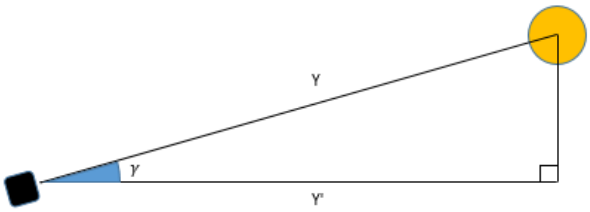

Fig. 14. Estimated distance from the angle of the camera

By tilting the camera, the depth becomes Y' instead of Y. Y' can be expressed using the angle (γ) of the servomotor and the depth Y obtained before tilting using (20).

$$\cos(\gamma) = \frac{Y'}{Y}$$

$$\Leftrightarrow \quad Y' = Y\cos(\gamma)$$

$$\Leftrightarrow \quad Y' = \frac{L}{-\tan(\alpha) + \tan(\beta)}\cos(\gamma) \tag{20}$$

Also, X' is

$$X' = \frac{L}{2} - Y'\tan(\alpha)$$

$$\Leftrightarrow \quad X' = \frac{L}{2} - \frac{L}{-\tan(\alpha) + \tan(\beta)}\cos(\gamma)\tan(\alpha) \tag{21}$$

From X' and Y', the angle (θ') from the center of the modified stereo camera to the object can be obtained by (22).

$$\tan(\theta') = \frac{X'}{Y'}$$

$$\theta' = \tan^{-1}\frac{X'}{Y'}$$

$$\theta' = \tan^{-1}\frac{\frac{L}{2} - \frac{L}{-\tan(\alpha) + \tan(\beta)}\cos(\gamma)\tan(\alpha)}{\frac{L}{-\tan(\alpha) + \tan(\beta)}\cos(\gamma)}$$

$$\theta' = \tan^{-1}\frac{-\tan(\alpha) + \tan(\beta) - 2\cos(\gamma)\tan(\alpha)}{2\cos(\gamma)} \tag{22}$$

From the above, the coordinates of the object when the camera is tilted up and down and the angle from the center of the stereo camera to the object can be derived.

D. Movement Control

The movement of the coaxial mobile robot is controlled using the distance and angle from the robot to the person measured by the stereo camera. The motor used to drive the wheels of a coaxial two-wheeled mobile robot does not have an encoder. Therefore, in this study, the coaxial mobile robot's movement sets the time for turning the motor. The rotation time of the motor was determined from the regularity due to time change by measuring multiple times. In addition, since the coaxial two-wheeled mobile robot can make a pivot turn that turns on the spot by rotating the left and right wheels in the opposite direction, the coaxial two-wheeled mobile robot is directed in the direction in which there is a person by this turning method. This turning is also performed by the rotation time of the motor as well as the amount of movement.

E. Experimental Design

There are four scenarios to test the control algorithm. In experiment I, the mobile robot moves to the target. The mobile robot moves to crowds in experiment II. In experiment III, the mobile robot moves to multiple targets. Finally, in experiment IV, the mobile robot autonomously moves around the outdoor environment.

III. RESULT AND DISCUSSION

A. Face detection using Circularity and Aspect Ration

As verification experiments, we measure circularity [47] and aspect ratio [51], set parameters, and measure distance with a stereo camera. A thermal image of a human face was acquired using a thermal camera, and the circularity was measured. When measuring a person's face, we stood in front of the camera in a stationary state. The results are shown in Table 3.

TABLE III. MEASUREMENT RESULTS OF CIRCULARITY AND ASPECT RATIO

Subject	Circularity	Aspect Ratio
A	0.7992	0.6250
B	0.7516	0.6591
C	0.7755	0.8205
D	0.8156	0.6136
E	0.7882	0.5517
F	0.7471	0.8000
G	0.7320	0.5652
H	0.8372	0.7179
I	0.6972	0.7353
J	0.7237	0.7813

As a result of measuring the circularity of the face, it was found that the roundness of the human face is often 0.7 or more. However, it may be a little low, such as subject I, with a circularity of 0.6972. This is because the shape of the face part acquired by the thermal image changes depending on the hairstyle and the like.

Therefore, we add a judgment method that considers circularity and the shape of the face. As a result of measuring

the aspect ratio of the face, none of them had an aspect ratio exceeding 1, but the difference between the minimum and maximum values is 0.2553. The reason for this is thought to be individual differences depending on the angle and system of the face. From this result, 0.5 to 0.9 is used as a human judgment for the aspect ratio. From this, human recognition is performed by setting the roundness of the face to 0.65 to 0.9 and the aspect ratio to 0.5 to 0.9.

B. Human Recognition Using Thermo Camera in Different Environments

As discussed in the preceding section, camera systems are affected by surrounding illuminance conditions. Therefore, we compare human recognition by the thermal camera proposed in this study and human recognition by the Viola-Jones method using a normal camera, which is the mainstream of face recognition [54], [55]. The environmental variations investigated were as follows:

a) Outdoors in the sun
b) Outdoors in the sun (backlit)
c) Outdoor shade
d) Outdoor shade (backlit)
e) When the lighting is bright indoors
f) When the lighting is dim indoors
g) When the lighting is off indoors
h) When people overlap
i) When a person and a hot object overlap

The left side of the figure is face recognized by a thermal camera, and the right side is face recognized by a Viola-Jones algorithm which is inbuilt in many commercial cameras. If human recognition is successful, it will be surrounded by a green border on a thermal camera and a yellow border on a normal camera. Figs. 15(a-i) show face recognition results in various environments. The measurement results at this time are summarized in Table 4.

TABLE IV. THE RESULT OF FACIAL RECOGNITION IN DIFFERENT ENVIRONMENTS

Experiment	Circularity	Aspect Ratio
A	○	○
B	○	△
C	○	×
D	○	×
E	○	○
F	○	△
G	○	×
H	△ (1 person only)	△ (1 person only)
I	×	○

In the measurement results, ○ is an evaluation that can be recognized stably, × is an evaluation that cannot be recognized, and △ is an evaluation that is not stable but can be recognized. In Experiment h, when people overlapped, only one person was recognized. In addition, it was confirmed that recognition by the thermal camera was impossible in Experiment I when it overlapped with a high-temperature object. From this result, it can be confirmed that the thermal camera can recognize the face stably with little influence from the illuminance and backlight of the environment. However, when the face overlaps with an object close to the temperature of the face or another person's face, the shape of the binarized image changes, and the face cannot be recognized. On the other hand, it was confirmed that in face recognition with a normal camera, the image becomes dark due to the influence of the illuminance and backlight of the environment, and stable face recognition cannot be performed.

From this, it can be seen that the proposed human recognition system is strong against changes in the illuminance of the environment and can show significance, but it cannot be recognized when the human face overlaps with a human face or a high-temperature object. Finally, it is necessary to verify the case where the temperature is high as a whole, such as under the scorching sun, which will be an issue in the future.

C. Distance measurement with fixed base

We varied the separation distance of servomotors and target object position to determine the ideal conditions for determining the target's distance. In the experiment, the separation distance of cameras varied between 0.2 – 1 m. Two target positions were chosen as (X,Y) = (-1, 2) m and (-1, 3) m.

First, as a preliminary experiment, the servomotor is attached to a fixed stand (desk). The cameras are positioned L = 0.2 m apart centered at (X, Y) = (0, 0). Two objects are introduced, as shown in Fig. 15. We recorded five readings of the same position as shown by measured points.

As can be seen from the graph in Fig. 16 and Table 5, the measured position deviated with an average error of 0.3 [m] and a standard deviation (std) of 0.3m from the actual standing position. It is possible that the cause of this is that the distance between the cameras is too close, and a slight angle shift has a large effect on the distance. Therefore, another experiment was conducted by increasing the distance between the cameras to cameras to 1 [m]. As seen from Table 5, when the L = 1 m, an error of 0.2 m is reported with std = 0.1 m, producing a more accurate measurement.

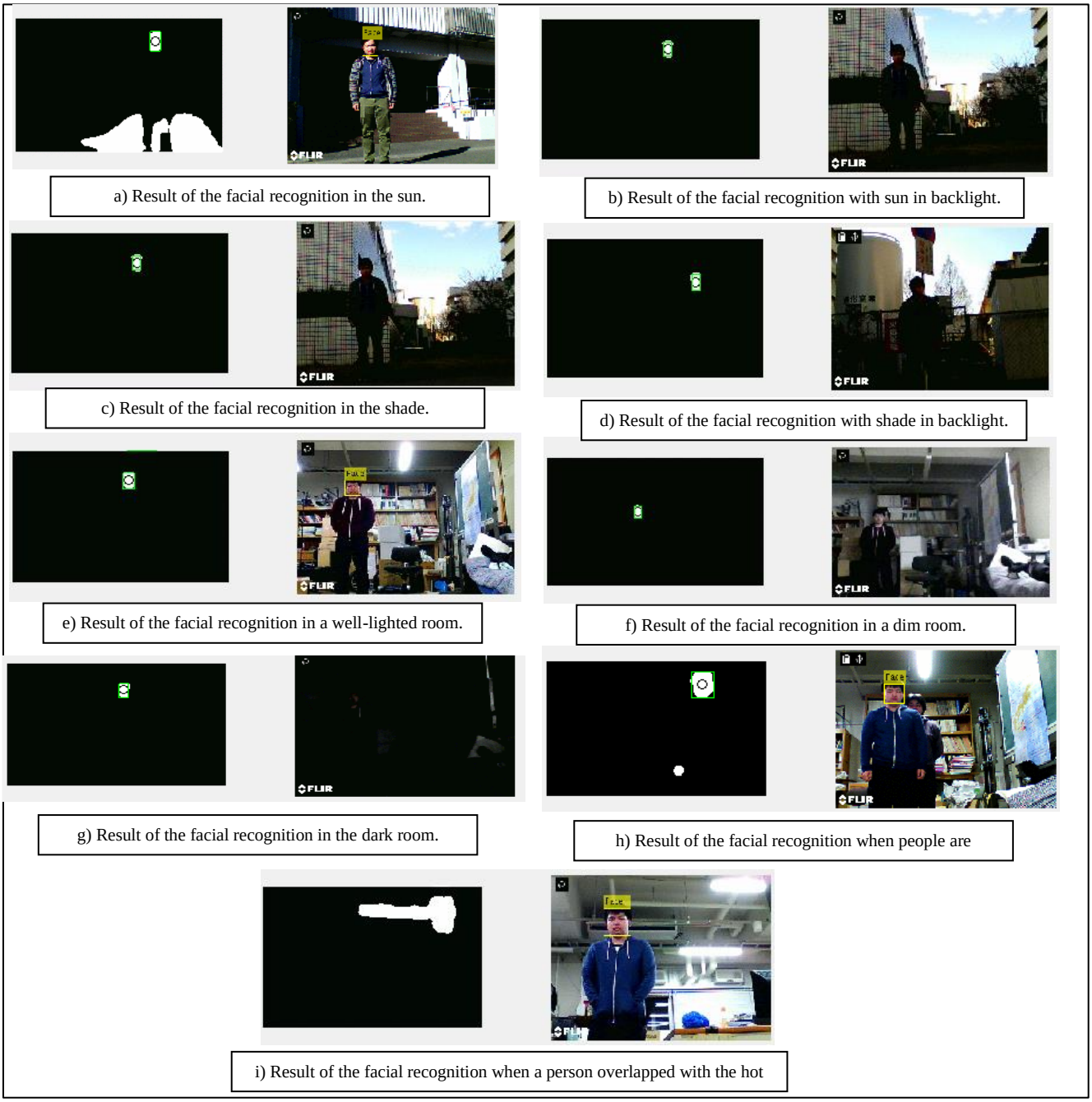

Fig. 15. Experiment results for different environmental conditions

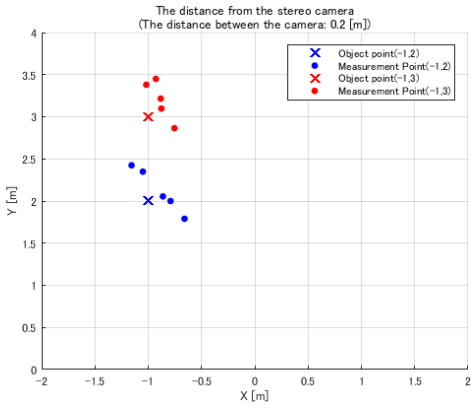

Fig. 16. Measurement of the distance from the stereo camera to the human. (L=0.2[m])

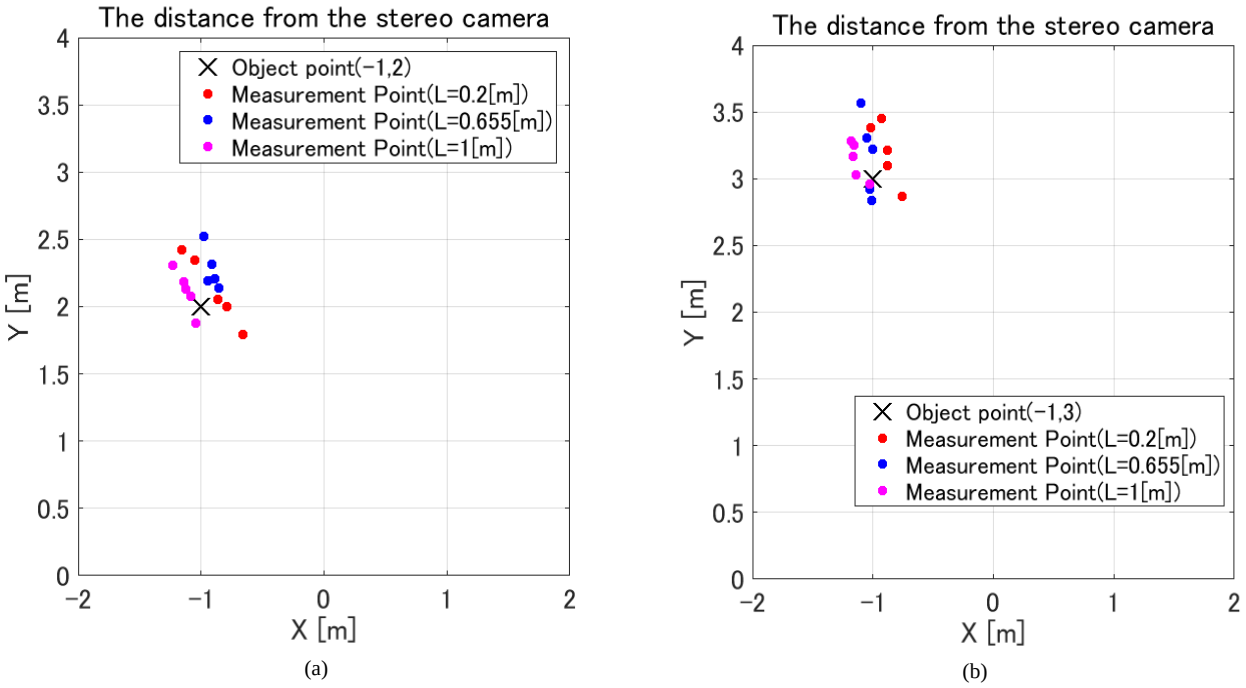

Fig. 17. Comparison of measurement of the distance from the stereo camera to the target (human) (a) object at (-1,2) and (b) object at (-1,3)

D. Distance measurement on a coaxial mobile robot

From the preliminary test, the distance between cameras should be as wide as possible, but due to hardware configurations, we could only get an L = 0.655 m between cameras when mounted on a coaxial mobile robot. The result of the distance measurement comparing the results of L=0.2, L=0.66, and L=1 m is shown in Fig. 17(a) and Fig. 17(b) and summarized in Table 5. From this, the distance between the cameras should be as wide as possible.

TABLE V. AVERAGE ERROR AND STANDARD DEVIATION OF THE MEASUREMENT RESULTS

	The distance between two cameras					
	0.2[m]		**0.655[m]**		**1[m]**	
Human Position (X,Y) **[m]**	-1,2	-1,3	-1,2	-1,3	-1,2	-1,3
Average error **[m]**	0.2658	0.2809	0.2973	0.2670	0.2076	0.2095
Standard deviation	0.2870	0.2225	0.1405	0.2582	0.1523	0.1301

E. Robot experimental results

In this section, we describe the overall results obtained. The experiment was conducted to capture the purpose of this research of human recognition and navigating autonomously to the target. In the setup, we conducted a running experiment assuming public relations activities (distributing pamphlets, measuring temperatures, helping with sanitization, etc.). The distance from the robot to the person is measured using the proposed system, and the robot is stopped 2 m in front of the person to avoid a collision. In this experiment, we asked the collaborators to stand with their faces raised as much as possible to obtain the correct distance. The running experiment is performed in the following four scenarios, each verifying a use case:

I. A person is standing in front of the robot.
II. A group of people and one person stand in front of the robot.
III. Attending to a sparse group following a track.
IV. A person standing outdoors in front of the robot

In summary, driving experiment, I recognized a person and approached the person stopping at a safe distance of 2 m from the target. Driving experiment II recognizes multiple people and is expected to move towards the crowd first. Driving experiment III identifies and follows a track to attend to all the targets (people). Experiment IV was conducted to verify the performance in an outdoor environment. The traveling track was monitored by LRF and reported herein to confirm the system performance.

Experiment I: Autonomous Movement to Target

The graphs below show the performance of the running experiments with various scenarios. In the graph, four states of the robot are indicated as Start, Move, Turn and Stop. The target (human) is shown in "X" at varying positions. The blue lines indicate the start position of the robot. The red plot is the robot turning state. The green plot is the robot moving. The purple plots show-stopping/stationary 2 [m] in front of a person. Yellow plots are nearby walls and objects.

Fig. 18 shows the layout and results of the running experiment I. The robot starts at (X, Y) = (0, 1) m, and the target is at (X, Y) = (-1, 4) m. The distance from the initial robot position to the target is estimated to be about 3.16 [m], and the angle is estimated to be about 18.4 [deg] using the camera system. The values measured by the stereo camera are shown in Table 6. As seen in Table 6, the difference between the true value and the measured value is about 0.15 [m] for the distance and about 0.8 [deg] for the angle. The robot moved to (X, Y) = (-0.5, 2) m and stopped as shown.

TABLE VI. THE DISTANCE AND ANGLE MEASUREMENT OF DRIVING TEST I.

	X[m]	Y[m]	Distance[m]	Theta[deg]
Actual value	-1.0000	3.0000	3.1623	18.4349
Measured value	-1.0046	3.1583	3.3143	17.6446

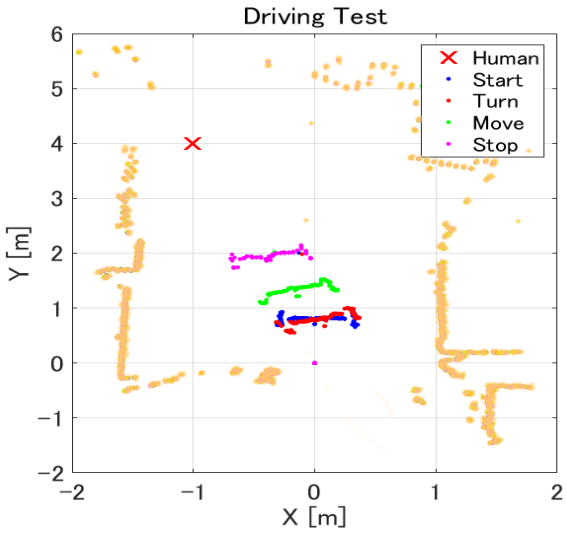

Fig. 18. Running locus of driving test I

Experiment II: Autonomous Movement to Crowds

Next, in order to verify whether the robot would move to the group, we conducted experiment II as shown in Fig. 19, with two people standing in front of the left and one person in front of the right of the robot. The number of people is determined by the number of center points of each face when performing face recognition. From the results in Fig. 19, it can be seen that the movement is toward the group.

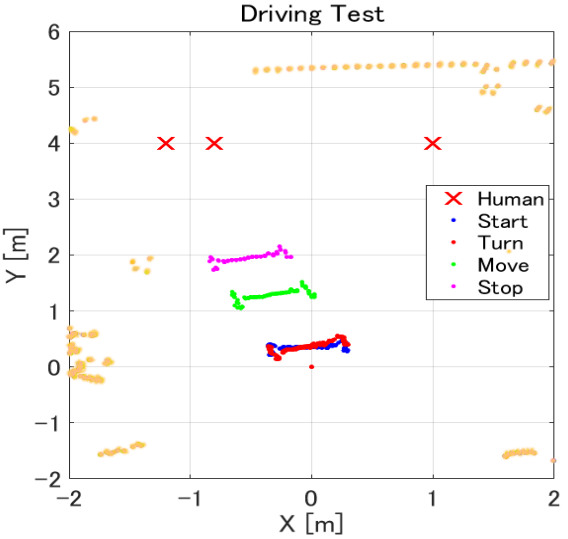

Fig. 19. Running locus of driving test II

Experiment III: Autonomous Movement to Multiple Targets

In practice, people are not stationary, and as such, tasks should be performed in a subsequent manner. In the third test run, we conducted the experiment assuming multiple targets that are spaced out in the environment. Each individual is attended to with a certain service period, after which the robot moves to the next target. As a means of attending to all the targets while following the specified route, the approximate angle of the person is obtained, the distance is measured, and the robot moves to the recognized person's location. In driving test III, if there are people at similar angles on the left and right, the person on the left is recognized first due to the flow of the program. The robot first stops at (X, Y) = (0, 0.5) m to attend to the target at (X, Y) = (-1, 3) m before proceeding to final stop at (X, Y) = (0, 3) m to attend to the target at (X, Y) = (1, 5) m as shown in Fig. 20. The initially measured values are shown in Table 7. From the table, the first target was near and located on the left and thus was given priority.

First, the coaxial mobile robot recognizes the person on the left and measures the distance and angle. After moving in front of the first target, the robot was able to search for a new target on the spot and head for the new target. From this, we searched for a person and succeeded in moving to an appropriate place.

TABLE VII. THE DISTANCE AND ANGLE MEASUREMENT OF DRIVING TEST III.

	First Target		Second Target	
	Distance[m]	Theta[deg]	Distance[m]	Theta[deg]
Actual value	3.1623	18.4349	4.135	-38.1146
Measured value	3.1273	18.759	3.6951	-35.7879

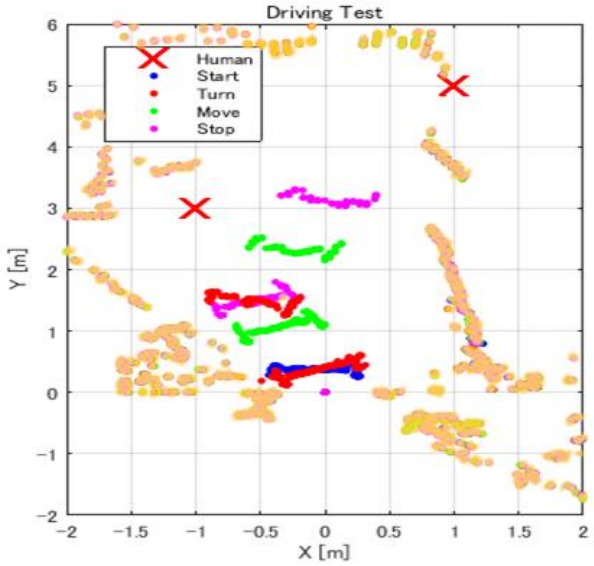

Fig. 20. Running locus of driving test III

Experiment IV: Autonomous Movement in Outdoor Environment

The previous experiments explored indoor scenes confirming the validity of the system. In this case, we investigated an outdoor environment that is seen as a challenge for the thermal camera due to sun rays. The experiment is conducted with a person standing at (X, Y) = (1, 4) m in front of the robot, as shown in Fig. 21. As seen in an outdoor environment, human recognition was also

successful as the robot followed the expected sequence of states and stopped as expected.

Through various scenarios, the system performance was confirmed with satisfactory robot movement. In addition, since the number of people could be grasped from the driving experiment II and moved in a large number of directions, it was confirmed that efficient movement is possible when assuming public relations activities. However, it can be seen that the distance accuracy is low through running experiments. It can be seen that the distance between cameras affects the decrease in distance accuracy as described in the experiment on the distance between cameras of stereo cameras. Regarding the angle from the robot to the recognized person, there is a difference of up to about 7 [deg] between the true value and the measured value, but the distance from the position where the robot stopped to the person is about 2 m. It is considered that there is no problem in conducting public relations activities that the inclination of the main body of the coaxial mobile robot has a deviation of 7 [deg].

In outdoor driving experiments, multiple objects were reflected in the thermal image, but we succeeded in distinguishing them by human recognition based on the circularity and aspect ratio. In addition, the coaxial two-wheeled robot may be strongly affected by the wind and other dynamic objects when traveling and may not be able to move to the correct position. Therefore, it is a future task to measure the distance in real-time. At the time being, distance measurement is conducted by the stereo camera system, and LRF is used to verify performance (plots) and is not integrated into the system.

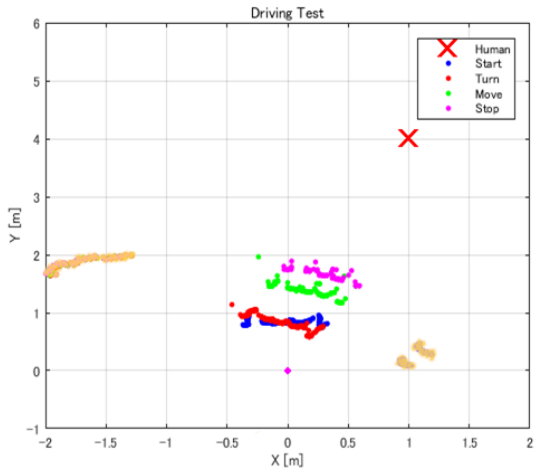

Fig. 21. Running locus of driving test IV

IV. CONCLUSION

We designed a human tracking system using a coaxial mobile robot based on a stereo thermal camera and confirmed autonomous maneuvering in multiple scenarios (use cases) as would apply in public relations. In human recognition, we succeeded in discriminating by the circularity and aspect ratio of the human face from thermal images. The circularity of the human face was found to be between 0.65 to 0.9 in the test subjects employed. To increase the discrimination of the target, we incorporated the face aspect ratio to improve the detection algorithm. From the verification results, the face recognition system was robust to environmental changes with successful discrimination in shadows, different lighting conditions, and dark places. The system fails to perform accurately when a person overlaps with another person or a hot object that mars the shape of the face.

In distance measurement, we utilized a steerable stereo camera using servo motors to deliver a wider sweep of the search path. This is a key to better performance compared to a fixed base, making it possible to search for a wide range of targets. From the verification results, we found that the wider camera separation distance gave better measurement accuracy. However, distance measurement using stereovision is inferior in distance accuracy compared to laser rangefinders. In this study, there is an error of about 0.3 m between the true value and the measured value. Therefore, improvement of the distance measurement function is required. The laser range finder has been mainly used for distance measurement in recent years, and the distance measurement accuracy is very high at the millimeter level. From this, it is considered that accurate distance measurement is possible by combining the angle from the robot to the stereo camera with measurements from LRF.

In addition, due to the characteristics of the coaxial mobile robot, it became clear during a running experiment that the robot body tilted when running or stopping, and the accurate angle in the height direction might not be measured. From this, it is considered that the center of gravity of the motion dynamics will affect the accuracy of readings. This should be considered to either counter the tilts and swings or perform recordings with the stabilized system. The downside to waiting would be on increased operation time.

Finally, we conducted running experiments with multiple scenarios and confirmed that we could recognize people and move the robot autonomously as expected. We confirmed that it was possible to operate both in indoor and outdoor environments with varying targets. However, since the distance is not measured in real-time, it was not possible to respond adaptively to changes in the environment like dynamic obstacles and disturbances such as wind. As a remedy, it is possible to improve performance by integrating LRF results to detect disturbance and react as the need arises.

As a future policy, with the drive-type stereo camera proposed in this research, it takes time to move a person to the center of the screen by driving a motor. It is necessary to increase the speed to use it as a public relations function. In addition, since it is necessary to improve the distance accuracy, it is required to use an LRF to speed up and improve the accuracy of distance measurement. As a method, it is possible to measure the angle and distance of a person by measuring the angle with a servomotor and the distance with a laser range finder by driving a laser that measures the distance on a straight line simultaneously as driving the camera. Alternatively, it is a method of measuring the angle/distance of a person by comparing the angle/distance information obtained from the laser range finder that scans the laser in the horizontal direction used for measuring the traveling locus with the angle of the servomotor. It is expected to solve this by performing human recognition with the thermal camera that proposed human recognition as

described above and using laser distance measurement for distance measurement.

ACKNOWLEDGMENT

This research is funded by the collaboration of the Faculty of Engineering, Gifu University, and the Electrical Engineering Department, Faculty of Engineering, Universitas Andalas.

REFERENCES

[1] A. Khan, B. Rinner, and A. Cavallaro, "Cooperative robots to observe moving targets: Review," *IEEE Trans. Cybern.*, vol. 48, no. 1, pp. 187–198, 2018, doi: 10.1109/TCYB.2016.2628161.

[2] K. P. Sinaga and M. S. Yang, "Unsupervised K-means clustering algorithm," *IEEE Access*, vol. 8, pp. 80716–80727, 2020, doi: 10.1109/ACCESS.2020.2988796.

[3] A. J. Abougarair and M. M. Edardar, "Adaptive Neural Networks Based Robust Output Feedback Control for Nonlinear System," *Wseas Trans. Comput. Res.*, vol. 9, no. 1, pp. 125–136, 2021, doi: 10.37394/232018.2021.9.15.

[4] A. Ouda and A. Mohamed, "Autonomous Fuzzy Heading Control for a Multi-Wheeled Combat Vehicle," *Int. J. Robot. Control Syst.*, vol. 1, no. 1, pp. 90–101, 2021, doi: 10.31763/ijrcs.v1i1.286.

[5] M. Tahmasebi, M. Gohari, and A. Emami, "An Autonomous Pesticide Sprayer Robot with a Color-based Vision System," *Int. J. Robot. Control Syst.*, vol. 2, no. 1, pp. 115–123, 2022, doi: 10.31763/ijrcs.v2i1.480.

[6] J. Smids, S. Nyholm, and H. Berkers, "Robots in the Workplace: a Threat to—or Opportunity for—Meaningful Work?," *Philos. Technol.*, vol. 33, no. 3, pp. 503–522, 2020, doi: 10.1007/s13347-019-00377-4.

[7] R. Tomari, Y. Kobayashi, and Y. Kuno, "Analysis of socially acceptable smart wheelchair navigation based on head cue information," *Procedia Comput. Sci.*, vol. 42, pp. 198–205, 2014, doi: 10.1016/j.procs.2014.11.052.

[8] G. D'Andréa, L. Bordenave, F. Nguyen, Y. Tao, V. Paleri, S. Temam, A. Moya-Plana, and P. Gorphe, "A prospective longitudinal study of quality of life in robotic-assisted salvage surgery for oropharyngeal cancer," *Eur. J. Surg. Oncol.*, vol. 48, no. 6, pp. 1243-1250, 2022, doi: 10.1016/j.ejso.2022.01.017.

[9] C. M. Song, H. S. Bang, H. G. Kim, H. J. Park, and K. Tae, "Health-related quality of life after transoral robotic thyroidectomy in papillary thyroid carcinoma," *Surg. (United States)*, vol. 170, no. 1, pp. 99–105, 2021, doi: 10.1016/j.surg.2021.02.042.

[10] R. R. Galin and R. V Meshcheryakov, "Human-robot interaction efficiency and human-robot collaboration," in *Robotics: Industry 4.0 Issues & New Intelligent Control Paradigms*, pp. 55–63, 2020.

[11] A. Dzedzickis, J. Subačiūtė-Žemaitienė, E. Šutinys, U. Samukaitė-Bubnienė, and V. Bučinskas, "Advanced Applications of Industrial Robotics: New Trends and Possibilities," *Applied Sciences*, vol. 12, no. 1. 2022, doi: 10.3390/app12010135.

[12] J. Zhang, R. Liu, K. Yin, Z. Wang, M. Gui, and S. Y. Chen, "Intelligent Collaborative Localization among Air-Ground Robots for Industrial Environment Perception," *IEEE Trans. Ind. Electron.*, vol. 66, no. 12, pp. 9673-9681, 2018, doi: 10.1109/TIE.2018.2880727.

[13] W. Sheng, A. Thobbi, and Y. Gu, "An Integrated Framework for Human-Robot Collaborative Manipulation," *IEEE Trans. Cybern.*, vol. 45, no. 10, pp. 2030–2041, 2015, doi: 10.1109/TCYB.2014.2363664.

[14] H. Xing, L. Shi, K. Tang, S. Guo, X. Hou, Y. Liu, H. Liu, and Y. Hu, "Robust RGB-D camera and IMU fusion-based cooperative and relative close-range localization for multiple turtle-inspired amphibious spherical robots," *J. Bionic Eng.*, vol. 16, no. 3, pp. 442–454, 2019.

[15] C. F. Juang, M. G. Lai, and W. T. Zeng, "Evolutionary Fuzzy Control and Navigation for Two Wheeled Robots Cooperatively Carrying an Object in Unknown Environments," *IEEE Trans. Cybern.*, vol. 45, no. 9, pp. 1731–1743, 2015, doi: 10.1109/TCYB.2014.2359966.

[16] J. W. Wang, Y. Guo, M. Fahad, and B. Bingham, "Dynamic Plume Tracking by Cooperative Robots," *IEEE/ASME Trans. Mechatronics*, vol. 24, no. 2, pp. 609–620, 2019, doi: 10.1109/TMECH.2019.2892292.

[17] S.-J. Chung and J.-J. E. Slotine, "Cooperative Robot Control and Concurrent Synchronization of Lagrangian Systems," *IEEE Trans. Robot.*, vol. 25, no. 3, pp. 686–700, 2009, doi: 10.1109/tro.2008.2014125.

[18] I. Hassani, I. Ergui, and C. Rekik, "Turning Point and Free Segments Strategies for Navigation of Wheeled Mobile Robot," *Int. J. Robot. Control Syst.*, vol. 2, no. 1, pp. 172–186, 2022, doi: 10.31763/ijrcs.v2i1.586.

[19] Y. Zou, C. Wen, M. Shan, and M. Guan, "An adaptive control strategy for indoor leader-following of wheeled mobile robot," *J. Franklin Inst.*, vol. 357, no. 4, pp. 2131–2148, 2020, doi: 10.1016/j.jfranklin.2019.11.054.

[20] D. Gu and K. S. Chen, "Design and performance evaluation of wiimote-based two-dimensional indoor localization systems for indoor mobile robot control," *Meas. J. Int. Meas. Confed.*, vol. 66, pp. 95–108, 2015, doi: 10.1016/j.measurement.2015.01.009.

[21] Y. Nakamori, Y. Hiroi, and A. Ito, "Multiple player detection and tracking method using a laser range finder for a robot that plays with human," *ROBOMECH J.*, vol. 5, no. 1, p. 25, 2018, doi: 10.1186/s40648-018-0122-x.

[22] P. T. Nguyen, S.-W. Yan, J.-F. Liao, and C.-H. Kuo, "Autonomous Mobile Robot Navigation in Sparse LiDAR Feature Environments," *Applied Sciences*, vol. 11, no. 13. 2021, doi: 10.3390/app11135963.

[23] H. Liu, J. Luo, P. Wu, S. Xie, and H. Li, "People detection and tracking using RGB-D cameras for mobile robots," *Int. J. Adv. Robot. Syst.*, vol. 13, no. 5, 2016, doi: 10.1177/1729881416657746.

[24] G. Du, S. Long, F. Li, and X. Huang, "Active Collision Avoidance for Human-Robot Interaction With UKF, Expert System, and Artificial Potential Field Method," *Frontiers in Robotics and AI*, vol. 5. 2018.

[25] B. K. Patle, G. Babu L, A. Pandey, D. R. K. Parhi, and A. Jagadeesh, "A review: On path planning strategies for navigation of mobile robot," *Def. Technol.*, vol. 15, no. 4, pp. 582–606, 2019, doi: 10.1016/j.dt.2019.04.011.

[26] U. Côtéallard *et al.*, "A Convolutional Neural Network for robotic arm guidance using sEMG based frequency-features," in *IEEE International Conference on Intelligent Robots and Systems*. 2016, pp. 2464–2470, doi: 10.1109/IROS.2016.7759384.

[27] W. Guan, S. Chen, S. Wen, Z. Tan, H. Song, and W. Hou, "High-Accuracy Robot Indoor Localization Scheme Based on Robot Operating System Using Visible Light Positioning," *IEEE Photonics J.*, vol. 12, no. 2, 2020, doi: 10.1109/JPHOT.2020.2981485.

[28] T. Kanda, D. F. Glas, M. Shiomi, and N. Hagita, "Abstracting peoples trajectories for social robots to proactively approach customers," *IEEE Trans. Robot.*, vol. 25, no. 6, pp. 1382–1396, 2009, doi: 10.1109/TRO.2009.2032969.

[29] S. Saunderson and G. Nejat, "Investigating Strategies for Robot Persuasion in Social Human-Robot Interaction," *IEEE Trans. Cybern.*, vol. 52, no. 1, pp. 641–653, 2022, doi: 10.1109/TCYB.2020.2987463.

[30] G. Song, K. Yin, Y. Zhou, and X. Cheng, "A surveillance robot with hopping capabilities for home security," *IEEE Trans. Consum. Electron.*, vol. 55, no. 4, pp. 2034–2039, 2009, doi: 10.1109/TCE.2009.5373766.

[31] J. N. K. Liu, M. Wang, and B. Feng, "iBotGuard: An internet-based intelligent robot security system using invariant face recognition against intruder," *IEEE Trans. Syst. Man Cybern. Part C Appl. Rev.*, vol. 35, no. 1, pp. 97–105, 2005, doi: 10.1109/TSMCC.2004.840051.

[32] M. Javaid, A. Haleem, A. Vaish, R. Vaishya, and K. P. Iyengar, "Robotics Applications in COVID-19: A Review," *J. Ind. Integr. Manag.*, vol. 5, no. 4, pp. 441–451, 2020, doi: 10.1142/S2424862220300033.

[33] S. Wang, K. Wang, R. Tang, J. Qiao, H. Liu, and Z. G. Hou, "Design of a Low-Cost Miniature Robot to Assist the COVID-19 Nasopharyngeal Swab Sampling," *IEEE Trans. Med. Robot. Bionics*, vol. 3, no. 1, pp. 289–293, 2021, doi: 10.1109/TMRB.2020.3036461.

[34] S. H. Alsamhi and B. Lee, "Blockchain-Empowered Multi-Robot Collaboration to Fight COVID-19 and Future Pandemics," *IEEE Access*, vol. 9, pp. 44173–44197, 2021, doi: 10.1109/ACCESS.2020.3032450.

[35] S. K. von Bueren, A. Burkart, A. Hueni, U. Rascher, M. P. Tuohy, and I. J. Yule, "Deploying four optical UAV-based sensors over grassland: challenges and limitations," *Biogeosciences*, vol. 12, no. 1, pp. 163–175, 2015, doi: 10.5194/bg-12-163-2015.

[36] M. O. A. Aqel, M. H. Marhaban, M. I. Saripan, and N. B. Ismail, "Review of visual odometry: types, approaches, challenges, and applications," *SpringerPlus*, vol. 5, no. 1, p. 1897, 2016, doi: 10.1186/s40064-016-3573-7.

[37] A. Leigh, J. Pineau, N. Olmedo, and H. Zhang, "Person tracking and following with 2D laser scanners," in *2015 IEEE International*

Conference on Robotics and Automation (ICRA), 2015, pp. 726–733, doi: 10.1109/ICRA.2015.7139259.

[38] E. Dorronzoro Zubiete *et al.*, "Evaluation of a Home Biomonitoring Autonomous Mobile Robot.," *Comput. Intell. Neurosci.*, vol. 2016, p. 9845816, 2016, doi: 10.1155/2016/9845816.

[39] Y. Hosoda, K. Yamamoto, R. Ichinose, S. Egawa, J. Tamamoto, and T. Tsubouchi, "Collision Avoidance Control of Human-Symbiotic Robot," *Trans. JAPAN Soc. Mech. Eng. Ser. C*, vol. 77, no. 775, pp. 1051–1061, 2011, doi: 10.1299/kikaic.77.1051.

[40] R. Ali, P. Yunfeng, A. Ali, H. Ali, N. Akhter, J. Ahmed, and A. Jalil, "Passive Autofocusing System for a Thermal Camera," *IEEE Access*, vol. 8, no. 1, pp. 130014–130022, 2020, doi: 10.1109/ACCESS.2020.3006356.

[41] T. E. Salem, D. Ibitayo, and B. R. Geil, "Validation of infrared camera thermal measurements on high-voltage power electronic components," *IEEE Trans. Instrum. Meas.*, vol. 56, no. 5, pp. 1973–1978, 2007, doi: 10.1109/TIM.2007.903590.

[42] E. Benli, Y. Motai, and J. Rogers, "Human Behavior-Based Target Tracking with an Omni-Directional Thermal Camera," *IEEE Trans. Cogn. Dev. Syst.*, vol. 11, no. 1, pp. 36–50, 2019, doi: 10.1109/TCDS.2017.2726356.

[43] A. K. Kashyap, D. R. Parhi, and A. Pandey, "Analysis of Hybrid Technique for Motion Planning of Humanoid NAO," *Int. J. Robot. Control Syst.*, vol. 1, no. 1, pp. 75–83, 2021, doi: 10.31763/ijrcs.v1i1.285.

[44] J. Wang, Q. Xue, L. Li, B. Liu, L. Huang, and Y. Chen, "Dynamic analysis of simple pendulum model under variable damping," *Alexandria Eng. J.*, vol. 61, no. 12, pp. 10563–10575, 2022, doi: 10.1016/j.aej.2022.03.064.

[45] M. Sasaki, E. Kunii, T. Uda, K. Matsushita, J. K. Muguro, bin M. S. A. Suhaimi, and W. Njeri, "Construction of an Environmental Map including Road Surface Classification Based on a Coaxial Two-Wheeled Robot," *J. Sustain. Res. Eng.*, vol. 5, no. 3, pp. 159 – 169, 2020.

[46] M. Khaled, A. Mohammed, M. S. Ibraheem, and R. Ali, "Balancing a Two Wheeled Robot," 2009.

[47] J. Chen and X. Bai, "Thermal face segmentation based on circular shortest path," *Infrared Phys. Technol.*, vol. 97, pp. 391–400, 2019, doi: 10.1016/j.infrared.2019.01.021.

[48] Z. H. Xie, L. J. Liu, X. Y. Wang, and C. Yang, "An iterative method with enhanced Laplacian-scaled thresholding for noise-robust compressive sensing magnetic resonance image reconstruction," *IEEE Access*, vol. 8, pp. 177021–177040, 2020, doi: 10.1109/ACCESS.2020.3027313.

[49] E. H. Houssein, M. M. Emam, and A. A. Ali, "An efficient multilevel thresholding segmentation method for thermography breast cancer imaging based on improved chimp optimization algorithm," *Expert Syst. Appl.*, vol. 185, p. 115651, 2021, doi: 10.1016/j.eswa.2021.115651.

[50] H. El Khoukhi, Y. Filali, A. Yahyaouy, M. A. Sabri, and A. Aarab, "A hardware implementation of OTSU thresholding method for skin cancer image segmentation," *2019 Int. Conf. Wirel. Technol. Embed. Intell. Syst. WITS 2019*, pp. 1–5, 2019, doi: 10.1109/WITS.2019.8723815.

[51] S. Umirzakova and T. K. Whangbo, "Detailed feature extraction network-based fine-grained face segmentation," *Knowledge-Based Syst.*, p. 109036, 2022, doi: 10.1016/j.knosys.2022.109036.

[52] M. S. Yang and K. P. Sinaga, "A feature-reduction multi-view k-means clustering algorithm," *IEEE Access*, vol. 7, pp. 114472–114486, 2019, doi: 10.1109/ACCESS.2019.2934179.

[53] K. P. Sinaga, I. Hussain, and M. S. Yang, "Entropy K-Means Clustering with Feature Reduction under Unknown Number of Clusters," *IEEE Access*, vol. 9, pp. 67736–67751, 2021, doi: 10.1109/ACCESS.2021.3077622.

[54] A. Elngar, A. El, R. Naeem, A. Essa, and Z. Shaaban, "The Viola-Jones Face Detection Algorithm Analysis: A Survey," Journal of Cybersecurity and Information Management (JCIM), vol. 6, pp. 85–95, Apr. 2021, doi: 10.5281/zenodo.4898039.

[55] T. Paul, U. A. Shammi, M. U. Ahmed, R. Rahman, S. Kobashi, and M. A. R. Ahad, "A Study on Face Detection Using Viola-Jones Algorithm in Various Backgrounds, Angles and Distances," *Int. J. Biomed. Soft Comput. Hum. Sci. Off. J. Biomed. Fuzzy Syst. Assoc.*, vol. 23, no. 1, pp. 27–36, 2018, doi: 10.24466/ijbschs.23.1_27.